Comparison of boundary-layer and field models for simulation of flow through multiple-row tidal fences

Luke S Blunden, William M J Batten, Matthew E Harrison and AbuBakr S Bahaj[1]

[1]University of Southampton, School of Civil Engineering and the Environment, University Road, SO17 1BJ, Southampton, UK

Abstract

A simple conceptual model of an array of tidal stream generators is a series of porous fences subject to flow in one direction, neglecting lateral velocity variations, but allowing for vertical velocity shear. In the far-wake of a fence deep inside the array, the flow might be expected to have reached an equilibrium, where the longitudinal pressure gradient is balanced by the drag of the fences and the friction on the sea-bed. This paper compares two approaches to estimating the downstream decrease in velocity in multiple-row tidal fences; firstly a simplified model using ideas from boundary layer theory previously applied to wind turbine arrays; second, a CFD simulation of the flow field around a ten-row array using a general purpose off-the-shelf RANS Finite Volume solver. The CFD simulations have been themselves compared with measurements gained in a laboratory flume.

Keywords: Tidal power, Tidal streams, CFD, Boundary layers

Nomenclature

A_r	=	Area of flow incident on fence/turbine	$= \zeta l_y l_z$ m^2
c_f	=	Sea-bed drag coefficient	$= \tau / \frac{1}{2}\rho U^2$
c_d	=	Fence/turbine drag coefficient	$= T / \frac{1}{2}\rho U^2 A_r$
g	=	Acceleration due to gravity	$= 9.81$ m/s^2
h	=	Depth of water	m
z_H	=	fence/turbine centroid height	m
κ	=	Von Kármán constant	$= 0.4$
L_x, L_y	=	Spacing of fence/turbine	m
l_r	=	Characteristic dimension of roughness element	m
l_y, l_z	=	Extent of fence/turbine in lateral and vertical	m
S_0	=	Negative of free-surface slope	$= -\partial Z / \partial x$
T	=	Drag on isolated turbine	N
U	=	Depth-averaged flow speed	m/s
u_*	=	Friction velocity	m/s
u	=	longitudinal flow velocity	m/s
x, y, z	=	Longitudinal, lateral and vertical coordinates	m
Z	=	Free surface elevation	m
z_0	=	Roughness length of sea-bed	m
λ	=	Area ratio	$= A_r / (L_x L_y)$
ν	=	Molecular kinematic viscosity	$= 1 \times 10^{-6}$ m^2/s
ρ	=	Density of fluid	$= 1 \times 10^3$ kg/m^3
σ_y	=	Width ratio	$= l_z / L_y$
τ	=	Frictional stress on sea bed	N/m^2
ζ	=	Shape factor	rectangle: $= 1$, circle: $= \pi/4$

Subscripts

$-$	=	Upstream of the leading edge of fence/turbine array
$+$	=	Far downstream of the leading edge of the array
H	=	Centroid of fence/turbine

© Proceedings of the 8th European Wave and Tidal Energy Conference, Uppsala, Sweden, 2009

1 Introduction

In this paper, a distributed roughness approach, taken previously in estimating speed deficit in large wind turbine arrays has been revisited in the context of tidal stream power generation. This work extends that described previously in [1] by deriving an expression for displacement height and velocity profile in the part of the water column above the turbines or fences.

In the first part of the paper the simplified distributed roughness model is described. The predictions made by the model are then compared with CFD simulations of a series of tidal fences, simulated by porous surfaces within the computational domain. The use of porous surfaces to simulate turbine generators has been justified to a certain extent in the context of wind turbine arrays, as the far wake of a wind turbine is largely determined by its thrust coefficient and the local turbulence intensity [2, 3, 4]. A tidal fence is a special case of an array of tidal stream turbines where the lateral spacing is as small as possible. Consequently, flow variations in the lateral direction may be ignored and the problem reduced to two dimensions, vertical and longitudinal.

1.1 Rationale

There are two reasons for considering a distributed roughness model:

1. To provide an equivalent added roughness value for the array, combining the effects of bed roughness, device spacing and drag on devices, suitable for coastal-scale numerical modelling. This is to enable modelling of the impacts of large arrays of tidal stream turbines on the wider flow regime.

2. To estimate the equilibrium velocity deficit in very large array. This is to enable estimation of power generation by the array compared to that of an isolated generator, which has been analyzed for the

general case of a tidal fence across a well-bounded channel [5], but remains an open problem for less well bounded situations. The equilibrium solution provides asymptotic values that may feed into future non-equilibrium finite-array models, in a similar manner to [6].

1.2 Simulation of tidal arrays using added roughness

A distributed roughness approach has been applied previously to specific geographic locations by Sutherland et al. [7] in the case of tidal flows in channels, and by Blunden and Bahaj [8] to headland-accelerated tidal flow. In the former, the drag coefficient was increased until the maximum power was dissipated through the increased friction. In the latter, values of drag coefficient and spacing of turbines within the array were assumed prior to modelling, and averaged over the affected elements in the model mesh. In neither case were taken into account the changes in spatially-averaged vertical velocity shear profile due to the change in momentum balance within the array. Bryden et al. [9] have considered energy extraction in a layered 3-D model for some idealized cases, using 80×80 m grid cells. However, their work was focused on single-row tidal fences in channels rather than representing multi-row arrays.

1.3 Rough-wall flow through obstacle arrays

The modelling of wind turbine arrays using distributed roughness has been informed by boundary layer micro-meteorology, which has developed in the context of measuring and predicting flows over crops, forests and urban landscapes. These are classed as rough-wall turbulent boundary layer flows; 'rough-wall' as the Reynolds number $u_* l_r / \nu$ based on the characteristic height of the roughness obstacles l_r is high enough to attain similarity and viscosity is irrelevant. For a comprehensive review of rough-wall boundary layer flow, see Raupach et al. [10]. According to a classic analysis, the flow profile (whether in the atmosphere or an open channel) is considered to consist of a roughness sublayer, influenced by the friction velocity and the properties of the roughness, and an outer layer, influenced by the friction velocity and the boundary layer thickness, but not the roughness properties. Between the two layers is an overlapping region that follows the well-known logarithmic profile:

$$\frac{u}{u_*} = \frac{1}{\kappa} \ln\left(\frac{z-d}{z_0}\right) \tag{1}$$

where the zero-plane displacement d is used as a parameter for adjusting the profile for a better logarithmic fit; physically it is equivalent to the mean level of momentum absorption [11]. The roughness sub-layer extends from the surface up to some multiple of the characteristic roughness obstacle size. However, all of the layers are only vaguely defined within the limits of experimental accuracy. For arrays of bluff-bodies such as cubes, or within forest canopies, measurements of the mean flow profile within the roughness sub-layer have been fitted to an empirical exponential profile, derived assuming a constant mixing length throughout the layer. Flow profiles through comparatively sparse arrays of porous obstacles have not received the same degree of experimental investigation.

Table 1: Variation of frontal area to plan area ratio λ with tidal stream turbine size and configuration. n is the number of rotors per generator unit

l_z (m)	A_r (m^2)	n	σ_x (L_x/l_z)	σ_y (L_y/l_z)	λ ($nA_r/(L_xL_y)$)
10	79	1	15	7.5	0.007
16	201	1	15	4	0.013
20	314	2	7.5	4	0.052
0.1	-	-	7.0	-	0.143

The key geometric parameter of an obstacle array has been found to be the ratio of projected frontal area of obstacles to the horizontal area, λ [10]. Values of λ for tidal stream turbine arrays might be expected to be in the range 0.005–0.05 and for tidal fences 0.05–0.15 (see Table 1), compared to 0.05–10 for flows over vegetation. It has been observed that in atmospheric flows over arrays of obstacles of various shapes and arrangements, that at low obstacle densities $\lambda < 0.2$, plots of z_0/l_r against λ collapse onto a linear relationship [10, 12].

1.4 Previous application of approach to large wind turbine arrays

Where boundary layer theory has been applied to wind turbines, in most cases, the velocity profile has been considered logarithmic over the entire planetary boundary layer down to the hub height of the rotor, with a single new roughness length describing the flow through the array compared to the flow in the undisturbed state. The 'gradient wind' at height was assumed constant, although the boundary layer thickness was allowed to vary in some cases. A difficulty arises with the momentum approach to this type of model in that the distribution of drag between friction (and possibly form drag if there are large-scale features) at the bed and the turbines is not known [13]. The energy approach is even more uncertain however as the rotor- and wake-generated turbulence production is also not known. Newman [14] assumed that the shear stress on the ground was constant i.e. no change from upstream to within the array. The new roughness length could then be calculated from the sum of the shear stress on the ground and the spatially-averaged drag on the turbines.

Frandsen [15] proposed dual logarithmic velocity profiles matching at hub height, noting that flow below hub height had been observed to be logarithmic within a wind turbine array. The 'gradient wind' was used to eliminate the roughness length in the upper layer. In the inner layer, deep within the outer planetary boundary layer, the bed roughness height was assumed to be known and the lower flow profile matched to the upper

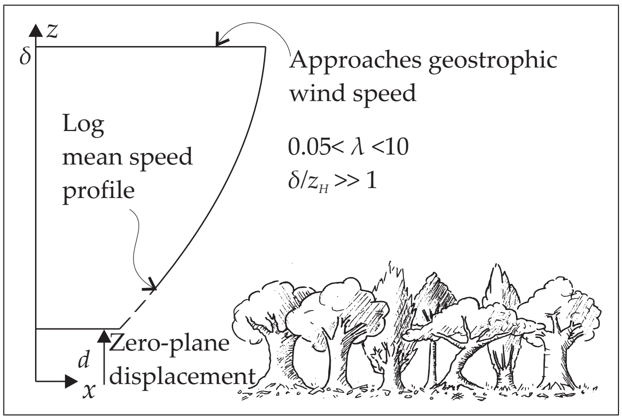

(a) Terrestrial canopy

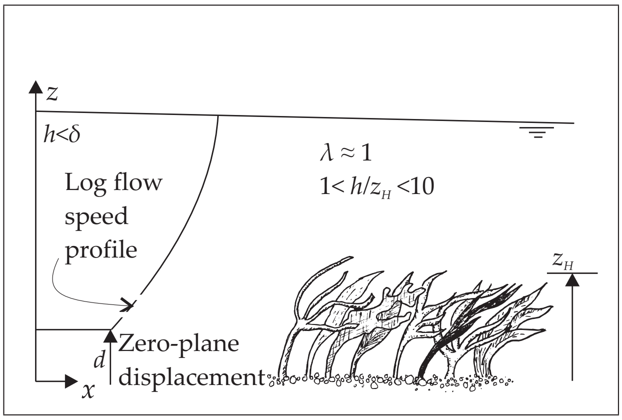

(b) Aquatic canopy

Figure 1: Conceptual models for flows over atmospheric and aquatic canopies

by velocity at hub height, resulting in a quadratic expression for hub height velocity.

The model of Frandsen bears similarities to the growth of a new internal boundary layer from the bed due to a change of bed roughness, where the upper layer retains the memory of the upstream roughness, whereas the slowly-growing internal layer is adapted to the new conditions. However, it is not clear why the internal layer would only extend to hub height and not grow to fill the whole external boundary layer. The velocity measurements cited by Frandsen as evidence of a logarithmic profile below hub height were taken within the onshore wind turbine array Nørrakær Enge II, Jutland, Denmark [16, page 27] where there were two to three points in the vertical below hub height and the measurements were taken at effectively two rows into the array. The measurements do not therefore represent conclusive evidence for the model being correct.

1.5 Similarities and differences with natural rough-wall flows through obstacle arrays

Definition sketches for different types of flow over obstacle roughness are included in Figure 1 and for flow through turbine arrays in Figure 2. The differences are apparent in terms of frontal area ratio and fraction of boundary layer or depth occupied by roughness height.

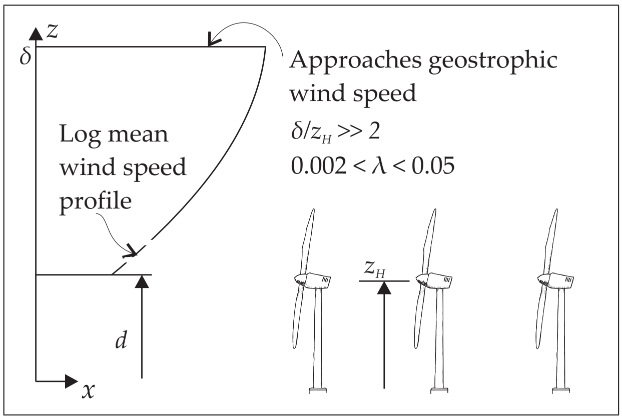

(a) Large wind turbine array after Frandsen [15] (density exaggerated)

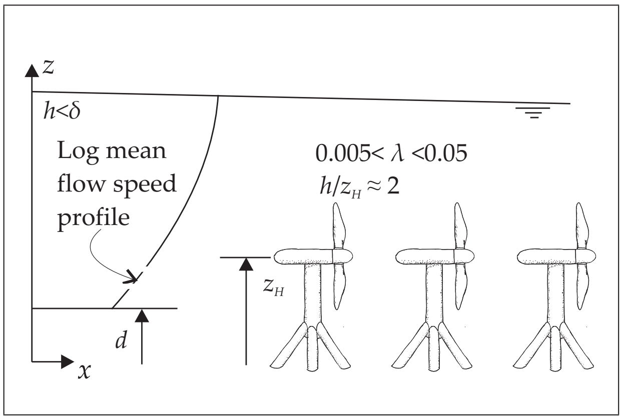

(b) Large tidal turbine array (density exaggerated)

Figure 2: Conceptual models for flow through wind and tidal turbine arrays

Flows through submerged vegetation bear the most resemblance to those in large tidal turbine arrays, in terms of fraction of depth of flow occupied. However, the high frontal area ratio in submerged vegetation results in a large zero-plane displacement in comparison to plant height, with a logarithmic profile above the canopy, observed in the laboratory with synthetic plants [17] and saltmarsh vegetation [18].

There is little experimental data for flow above and especially below the geometric roughness height of large arrays of obstacles of a similar nature to tidal turbines (low frontal area ratio, large fraction of depth occupied, high porosity, no flow separation) for comparison, although work has begun in this area [19]. MacDonald [20] investigated flow among and above arrays of cuboid obstacles and derived a semi-empirical exponential expression for the velocity profile below the obstacle height. In doing so, it was assumed that at each height above the surface, the drag coefficient experienced by the flow was constant and that the length scale for the turbulent viscosity was also constant. Moreover the lowest value of area ratio investigated was at the upper end of the range that might be expected for a tidal turbine array. Bentham and Britter [21] proposed an even simpler model, with the velocity constant below obstacle height. This gives results similar to [20] for low values of area ratio, and was proposed by in the context of modelling flow through and over urban canopies.

1.6 Vertical velocity profiles in fast tidal streams

The shape of the vertical velocity profile in a tidal stream varies over the tidal cycle, with phase differences in velocity over the water column as the upper portion is more affected by inertia and the lower by friction at the bed. These phase differences are most important when the velocities are low and are therefore likely to have little effect on the energy capture of a tidal turbine, which would be generating at low efficiency or not at all (if below cut-in speed). The external balance of forces in the tidal stream when flowing strongly is between the longitudinal pressure gradient due to sea-surface slope and frictional stresses on the sea bed. There are 'spikes' in the inertial acceleration term around slack water, but otherwise this term makes a small contribution to the momentum balance [22].

Observations made in a moderately fast tidal stream of amplitude 1.2 m/s in depth of around 50 m [23] indicated a good fit to a logarithmic profile over most or all of the depth sampled (30–40 m above the bed) during the ebb and flood periods. In a fast, unstratified tidal stream, the logarithmic profile may extend all the way to the free surface [24]. There is no free-stream as such and the entire flow 'feels' the roughness. In the atmosphere by contrast, the vertical extent of the boundary layer is much larger (in comparison to the obstacle size or turbine hub height), and conditions approach a free-stream wind-speed which is considered essentially fixed by external conditions.

The upper part of the water column close to the surface is avoided by most designs of full-scale tidal stream turbine rotor assembly, for many reasons including cavitation or ventilation on the blade tips; hazards to surface vessels and wave action. Consequently deviation of the velocity profile from logarithmic in the outer region is unlikely to have a large effect on the predicted incident resource in the natural state.

In conclusion, the evidence above implies that it is reasonable to expect that the tidal flow in the natural state is fully rough-turbulent and the mean vertical velocity profile can be described by a logarithmic function over most of the depth (from close to the roughness to close to the surface).

2 Distributed roughness model for a large tidal stream turbine array

The following part of this paper details a new model which extends the methodology previously used for wind turbine arrays, to tidal stream arrays. The mean velocity profile above the fences is derived based on a logarithmic function. In order to develop the new model, two further assumptions need to be made.

Assumption 1 *The force upon and power generated by each unit depends only on the mean incident velocity at the hub height (or at the height of the centroid of the swept area of the turbine).*

This assumption neglects non-linearities in the vertical velocity profile (and its higher moments, u^2 and u^3) upstream of the turbine rotor disk, that would be likely to lead to higher rotor-area-averaged characteristic velocities for drag and power than the centroid velocity. It would be possible to use multiple-streamtubes with varying velocities to integrate the profile across the swept area, but as the upstream velocity profile is not known in advance, this would lead to unjustifiable complication. Moreover, if the velocity profile maintains a similar form, values of c_d and c_P will be out by constant factors that may be established later in the light of experimental velocity profiles.

In reality, there would also be a contribution to the total drag experienced by the flow, caused by the structure providing reaction against the thrust of the turbine. This could be added into the model at a later stage based on the estimated drag on a particular structural configuration.

Assumption 2 *The flow within the array can be considered to be a sum of a mean value plus periodic components with period L_x.*

This assumption relies on the turbulent mixing deep within the array being sufficient that the mean flow adjusts to the new combined roughness of the array and the bed, so that there is no further change in drag on the turbines or friction on the bed with the stream wise coordinate, when averaged over subsequent periods of L_x downstream of the leading edge of the array.

A true finite-array added roughness model would need to take into account the non-equilibrium growth of an internal boundary layer from the leading edge of the tidal stream turbine array. Similarly, downstream of the array, the flow will require a certain distance to re-attain equilibrium. Parameters derived for an infinite array may be applied to a finite array in a similar manner to a standard assumption in open channel hydraulics, that a coefficient of friction derived for uniform flow can be applied to spatially-varied flow [25, page 217]. As the number of rows in the array increase, the edge-effects should diminish in importance and the solution converge on the case of an infinite array.

2.1 Hub height velocity within the large array

Under these assumptions, the velocity above the fences, several rows into the turbine array can be expressed as:

$$\frac{u_+}{u_{*+}} = \frac{1}{\kappa} \ln\left(\frac{z-d_+}{z_{0+}}\right) \tag{2}$$

There are three unknown variables: the friction velocity u_{*+}, the zero-plane displacement d_+ and the roughness length for the large array, z_{0+}. By analogy with flow over submerged vegetation, where it is assumed that $z=d$ is effectively a lower boundary to the flow and $h-d$ is the effective depth [17], the friction velocity can be related to the streamwise free surface slope by:

$$u_{*+} = \sqrt{gS_{0+}(h-d_+)} \tag{3}$$

Where $S_{0+} = -\partial Z/\partial x$. The free-surface slope (pressure gradient) S_{0+} is not known; for a finite array, it will be a function of upstream and downstream conditions. In addition it may be affected by the geometry of the array and the proximity of lateral boundaries. Assuming a fixed free-surface slope gives the most pessimistic estimate and the fixed flow-rate the most optimistic. Reality will lie somewhere between the extremes of constant slope and constant flow rate, i.e. the flow is likely to back-up in front of the array resulting in a local steepening of the free-surface slope across the array in the streamwise direction, but there will also be a local decrease in the depth averaged velocity.

u_{*+} is also known independently through the sum of the resistive forces, assuming equilibrium:

$$u_{*+} = \frac{1}{\sqrt{2}}\sqrt{c_d\lambda U_+^2 + \alpha c_{f-}U_-^2} \tag{4}$$

where

$$\alpha = \frac{c_{f+}U_+^2}{c_{f-}U_-^2} \tag{5}$$

If $\alpha = 1$, then there is no change in drag on the sea-bed with respect to the undisturbed case. When the free-surface slope is assumed constant and as $\lambda \to \{0, \infty\}$, $\alpha \to \{1, 0\}$, but for intermediate values of λ, α would depend on the distribution of shear stresses in the flow between the sea-bed and hub-height. For the previous wind turbine array models, authors have taken $\alpha \propto (u_{H+}/u_{H-})^2$ [13]. This is attractive as an approach as it links the upper and lower velocity profiles together, but is only valid where the velocity profile decreases monotonically to the bed. An alternative approach is adopted here: typical in marine applications, the friction coefficient is related to the flow velocity at 1 m above the bottom, u_{100} (10 mm in the 1/100 scale model). In the absence of any better information, the constant of proportionality is taken as unity:

$$\alpha = (u_{100+}/u_{100-})^2 \tag{6}$$

If there is acceleration of the flow underneath the fence then there is the possibility of an *increase* in bed friction inside the array. This will be discussed later in the light of the CFD model results (§5.2). The zero-plane displacement d, as mentioned previously, is the mean level of momentum absorption. It is often ignored for flow over surfaces as it is of the same order as the height of the roughness elements, i.e. $d_- \approx 0$ and consequently small compared to the depth. However, in the case of an obstacle array it may be raised significantly. The wind turbine models considered previously have assumed a zero-plane displacement of zero, presumably either for the sake of simplicity—it introduces awkward algebra into the expressions—or because the turbine hub height was much less than the thickness of the planetary boundary layer. Deep within the array, then mean level of momentum absorption may be estimated as:

$$\frac{d_+}{z_H} = \frac{\lambda c_d U_+^2}{\lambda c_d U_+^2 + \alpha c_{f-}U_-^2} \tag{7}$$

(a) Fixing arrangements. (b) Front view showing end discs to minimize vortices shed from ends.

Figure 3: Porous fence arrangement

with the requirement that $(z_H - d_+)/z_{0+} > 1$. The drag coefficient of the fences/turbines c_d is here referred to the local depth-averaged velocity.

In order to estimate the roughness length z_{0+}, reference must be made to the literature for rough-wall flow through obstacles. an empirical fit to data cited in [26] gives:

$$z_0/l_r = 0.5\lambda \tag{8}$$

Where l_r is the height of the roughness elements. In the case of the porous fences it is not clear what height corresponds to l_r as there is flow underneath a fence; the possible choices are the fence height l_z, the centroid height z_H or the total height $z_H + l_z/2$.

At this point u_{*+}, d_+ and z_{0+} are all specified providing α can be estimated; here the CFD results (§5.2) will be used to determine c_d and c_{f+}.

3 Physical model of four-row fence array

An array of four mesh fences was installed in a flume to simulate rows of tidal stream turbines with close lateral spacing. The experimental method and results are included here to compare with the CFD model in §4. The results have been presented previously in [27]. The measurements were carried out at the University of Southampton Chilworth Research Laboratory. The flume is 1.37 m wide and 21 m in length. For these measurements the flume was run at 0.3 m depth ($3l_z$), with a mean inlet velocity of 0.23 m/s. The geometric scaling of the experiments was 1/100 compared to a 10 m high fence in 30 m channel. Scaling the flow speed with channel Froude number gives a full-scale tidal speed of approximately 2.5 m/s. The Reynolds number based on the fence height, calculated at 3×10^5 is lower than full scale, but still within the fully turbulent range.

Four identical fences were constructed from a wire mesh, with width l_y of 0.95 m, height l_z of 0.1 m and longitudinal spacing L_x of 0.7 m and therefore $\lambda = 1/7$. At either end of the fence end discs were fitted (with diameter twice the height of the fence) to reduce edge effects. Fences were installed at the centre of the flume depth, with the midpoint at 0.15 m (1.5 l_z). A 10 N load cell was used to measure the reaction of the supporting arm, and allow the thrust coefficient of the fence assembly to be calculated. Measurements were made over a period of approximately five minutes. The fence arrangement is shown in Figure 3.

The data from the load cells were used to calculate

c_d:

$$c_d = T/(\frac{1}{2}\rho U_0^2 A_r) \tag{9}$$

Where U_0 is the undisturbed velocity at the first fence row. The measured voltages were translated to thrust values based on a calibration curve for the load cell, and moments around the pivot point for the supporting arm.

An Acoustic Doppler Velocimeter (ADV) was used to profile the flow velocity around the fences. It has been shown that mean velocity errors of less than 1% are achievable with this equipment [28]. A three-minute sample was made at each measurement location, at a sample rate of 50 Hz. Measurements were made at 3, 5, 7, 9, 11, 15, 20 and 25 l_z behind each fence, with eight measurements made vertically through the water column at each location. In the depth-wise direction, the measurement spacing was 10% of the depth i.e. 0.03 m. It was not possible to measure at 0%, 90% or 100% depth due to the limitations of the ADV methodology. At each fence location (with the fence removed) measurements were made at the centroid of the fence and $\pm 4.5 l_z$ laterally for an average velocity across the fence. The velocity behind each fence was profiled individually, such that data exists for the flow behind 1-, 2-, 3- and 4-fence configurations. A total of 328 measurements were made, each of duration three minutes.

4 CFD model of a ten-row tidal fence array

In this section the methodology is described for the computational model of a finite array of tidal fences. A tidal fence may be regarded as a close-packed row of tidal turbines (i.e. $\sigma_y \to \infty$). The array was represented by a series of porous surfaces in a channel. The results using the CFD methodology are then compared with experimental results (§5.1) in order to show the degree of agreement.

4.1 Computational method

The porous fences were spaced at $7 l_z$ ($l_z = 0.1$ m) apart and were modelled as sub domains, with the porous loss modelled as a directional momentum loss. The resistance loss coefficient was calculated using Equation 10. The value was then iterated until the measured pressure drop across one fence in the solution was similar to that measured in the flume.

$$c_d = C_R \Delta x \tag{10}$$

Where Δx is the thickness of the fence, and C_R is the resistance coefficient.

The domain was modelled at the same scale as the experiments (see §3), but with configurations of up to ten fences. The problem dimensions are shown in Figure 4. The inlet velocity profile in the experiments fell into either the smooth or transitional categories of hydraulic roughness, depending on the value of geometric roughness height assumed. Therefore, the velocity at the inlet boundary was defined by fitting a smooth-turbulent

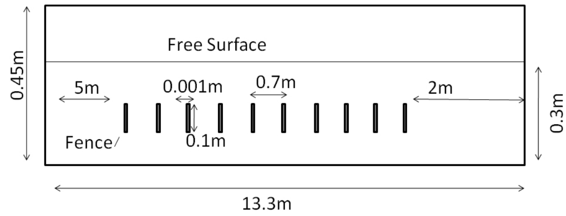

Figure 4: CFD problem geometry

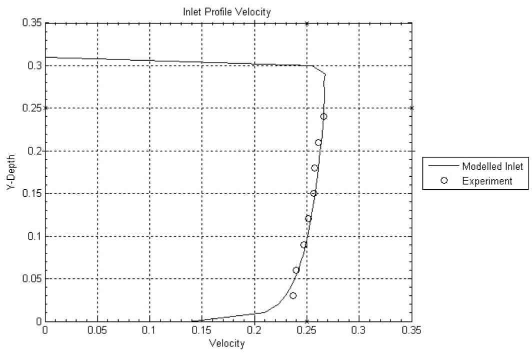

Figure 5: Inlet velocity profile

logarithmic profile (11) [24] to the measured data from the experiments.

$$u_{\text{in}} = \frac{1}{\kappa} u_* \ln\left(\frac{u_* z}{\nu}\right) + A \tag{11}$$

Where u_{in} is the modelled inlet velocity, u_* the friction velocity and A an arbitrary constant. Curve-fitting gave $u_* = 0.0070$ m/s and $A = 0.14$ m/s; the velocity profile was entered in CFX Expression Language (CEL) for the inlet boundary. The model inlet profile is shown with the measured points in Figure 5. The pressure at the outlet boundary was estimated by subtracting the pressure drop (in terms of static head loss) across the fences derived using open channel hydraulics. A head loss of 0.0054 m was estimated across ten fences with $c_d \approx 0.63$, and a hydrostatic pressure profile was set at the outlet based on this value (as an initial condition). This pressure value was used for all fence configurations. Assuming that most of the head loss occurred over the part of the channel containing the fences, the imposed head loss gave a friction velocity of approximately $u_* = 0.048$ m/s. Boundary conditions and other model parameters are summarized in Table 2.

The model calculations were made using ANSYS® CFX 11 Academic Research [29], which solves the Reynolds-Averaged Navier-Stokes (RANS) mass and momentum equations. CFX uses a hybrid finite-element/finite-volume discretization approach, which supports arbitrary mesh topology. Advection fluxes were evaluated using the second-order high resolution scheme.

For engineering applications, two-equation models have been most widely to model turbulence. They have

Table 2: CFD model parameters

Parameter	Setting
Water	Incompressible fluid
Air	Ideal Gas
Multi-phase Control	Homogeneous coupled free surface
Turbulence Model	SST
Inlet	Boundary layer model. See Figure 5. Free surface height 0.3 m
Bottom Boundary	No Slip Condition Smooth Wall
Sides Boundaries	Symmetry
Outlet	Static pressure 0 Pa, Free surface height $(0.3-0.0054)$ m
Top	Opening, Air, 0 Pa
Convergence criteria	RMS residual 1×10^{-6}

sufficient flexibility for modelling a variety of flows, at modest computational expense. The k-ε model is known to be insensitive to inlet turbulence intensity, but behaves poorly close to boundaries. The k-ω model by contrast, performs well close to boundaries but is sensitive to the specification of inlet turbulence intensity. A blended combination of the two models was proposed by Menter [30] to capture the best of both. This model was chosen for turbulence closure in the simulation.

A coupled volume-fraction algorithm was used to solve the free surface. The problem was defined in 2-D, in order to solve the XY plane behind the fences. In CFX, 2-D problems are modelled using a 3-D mesh of single element thickness.

4.2 Mesh refinement study

The basic mesh was a structured hexahedral arrangement, consisting of 2.66×10^5 nodes, and 1.32×10^5 elements. The CFX mesh adaptation system was used to refine the mesh in areas where the velocity gradients were high. Three mesh adaptation steps were undertaken for each model, with a node factor of 3.0 (i.e. the final mesh had around three times more nodes than the original). A sample of the basic and adapted mesh is shown in Figure 6, which shows that nodes were added in the wake region, and at the bottom boundary. Basic mesh values were chosen to ensure wall $20 \leq z_+ \leq 100$ giving good boundary layer resolution.

A mesh refinement study across the four meshes (basic mesh plus three successive adaptation steps) showed that the c_d modelled across the fences demonstrated convergence with increasing refinement. Table 3 shows the c_d values for each fence, at each adaptation step.

5 Results and Discussion

5.1 Experimental results

Figure 7 shows reasonable agreement between measured and modelled velocities on the fence centre-line. This gives a degree of confidence that the CFD model can reproduce the velocity deficit on the centre-line behind a ten fence array. It should be emphasized that each set of measurements was separate, e.g. one set made be-

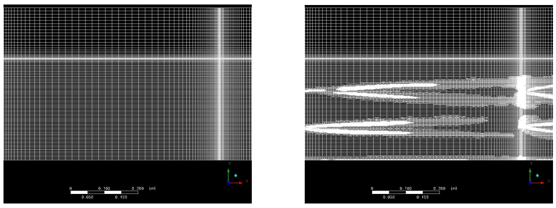

(a) Initial structured mesh. (b) Mesh after refinement

Figure 6: Adaptive meshing

hind one fence only, another behind two fences only and so on. Figure 8 shows that the agreement between modelled and measured velocity profiles measured above the centre-line was also reasonable but below the fences was poor. The region below the fences is of particular interest from the point of view of distributed roughness modelling, in order to determine the partition of resistance to the flow between the bottom and the fences. Consequently, further experiments are required to determine how the velocity profile varies with different gap heights $z_H - l_z/2$ and bottom roughness.

Tidal fences are a special case of tidal stream generator array; whereas the wakes of individual generators in a sparser array are able to expand and mix in the lateral direction, the wake of a tidal fence cannot. Continuity requires that there must be acceleration in a vertical plane above and/or below the porous fence. In contrast with the porous fence experiments, similar experiments with single isolated porous disks in a channel indicated that acceleration beneath the disks was insignificant [19, 31].

As mentioned in §4.1, the flow profile in the flume (upstream of the fences) either fell into the category of hydraulically-smooth or transitional. However, at full-scale the flow would fall into the hydraulically-rough category, with the simpler logarithmic velocity profile independent of wall Reynolds number. Introduction of artificial roughness on the bottom of the flume would be desirable for future experiments in order to bring the flow into the fully rough-turbulent regime. It would also be desirable to measure the pressure gradient directly; this is likely to be very small and in a laboratory may require special head amplification techniques for accurate measurement.

5.2 CFD results

Figure 9 shows that the CFD model predicts an increase in friction coefficient downstream of the leading edge of the array, which has not fully converged after ten rows. The raw bed shear stress is noisy (is related to the velocity gradient at the bed) and is clearly sensitive to the discretization of the mesh. An empirical build-up exponential curve was fitted to the smoothed results in order to estimate the equilibrium value which gave $c_f = 0.00873$ with a 95% confidence interval of 5×10^{-5}. The curve fit predicted convergence to within 1% of the final value by a distance equivalent to fifteen fences deep into the array. Figure 10 shows the modelled drag coefficient of the porous fences multiplied by

Table 3: Thrust coefficient of each porous fence derived from model results. Thrust coefficient has been normalized by flow speed upstream of the first fence

Mesh	Number of:		Thrust coefficient c_d at fence number:									
	Nodes	Elements	1	2	3	4	5	6	7	8	9	10
Basic mesh	2.7×10^5	1.3×10^5	0.76	0.49	0.45	0.48	0.50	0.53	0.55	0.56	0.56	0.57
Refinement 1	5.1×10^5	3.7×10^5	0.76	0.50	0.46	0.48	0.51	0.53	0.55	0.56	0.56	0.57
Refinement 2	6.5×10^5	5.8×10^5	0.76	0.50	0.47	0.49	0.52	0.54	0.56	0.57	0.58	0.58
Refinement 3	8.2×10^5	8.0×10^5	0.75	0.50	0.47	0.48	0.51	0.54	0.55	0.56	0.57	0.57

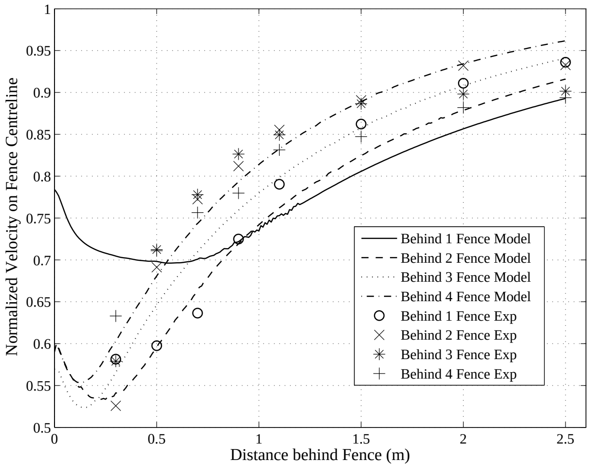

Figure 7: Comparison of experimental and modelled longitudinal velocity variation behind one to four fence arrays

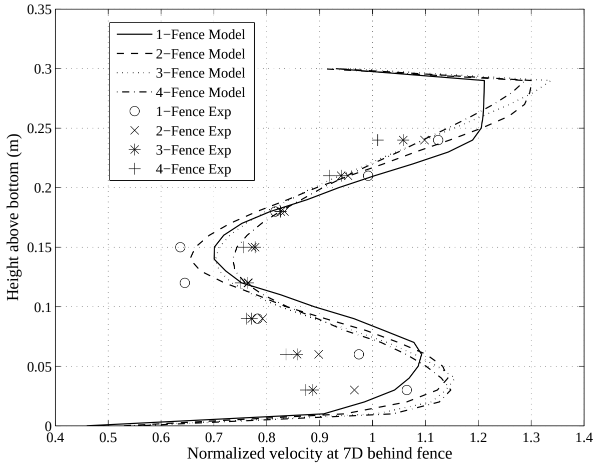

Figure 8: Comparison of experimental and modelled vertical velocity profiles behind one to four fence arrays, at $7l_z$ downstream.

the area ratio λ, indicating convergence. The values may then be compared directly with those in Figure 9 and it is immediately clear that in case the area-averaged fence drag is larger than bottom friction by a factor of ten, a result of the smooth bed and large λ.

5.3 Simplified model

Using the equilibrium values for friction and drag coefficient, values for the zero-plane displacement and friction velocity may be calculated using Equations (7) and (4), giving $d_+ = 0.137$ m and $u_{*+} = 0.0575$ m/s. For comparison, using (3), the imposed head drop in the model of 0.0054 m implies an average friction velocity over all the fences of $u_* = 0.0476$ m/s. Using the total height of the fence above the bottom as the appropriate length for Equation (8) gives $z_{0+} = 0.0142$ m. Based on these parameters, the velocity profile for $z \geq z_H + l_z/2$ may be plotted. Figure 11 shows the predicted profile along with those taken from three sections along the channel in the CFD results. It can be seen that the predicted profile lies in the same range of values as the CFD results but shows some differences in form. This new model has been based on both previous theories applied to wind turbine arrays and analogies with rough-wall boundary layer obstacle flows, in particular that over submerged vegetation. In the latter, obstacle densities are in general much higher and flow separation around obstacles occurs. In the former, arbitrary assumptions are made concerning the distribution of drag in the vertical. Consequently, the new model should be regarded as a tentative first step towards characterizing flow in large tidal arrays, highlighting the need for suitable experimental data for comparison.

Apart from λ, other geometric ratios such as lateral and longitudinal spacing and areal blockage may be important in determining the equilibrium drag and velocity profiles for an infinite array, but their inclusion in a distributed roughness model would be at the expense of simplicity and currently without sufficient experimental data to compare.

The results of the previous equilibrium models applied to wind turbine arrays have indicated that they tend to give pessimistic estimates of the array efficiency when compared to experimental data [3] and empirical finite array models [13, 32].

6 Conclusions

1. A new model has been proposed for the velocity profile above a large array of tidal stream turbines. An important difference between this model and previous models is the inclusion of the upward displacement of the spatially-averaged mean level of the momentum absorption, the zero-plane displacement d, significant for plausible array densities.

2. A set of experiments were carried out on an array of four porous mesh fences in a channel. Measurements were made of flow velocities and drag on the fences. The results were compared with those of a CFD model with similar geometry and with the fences represented as imposed pressure gradients.

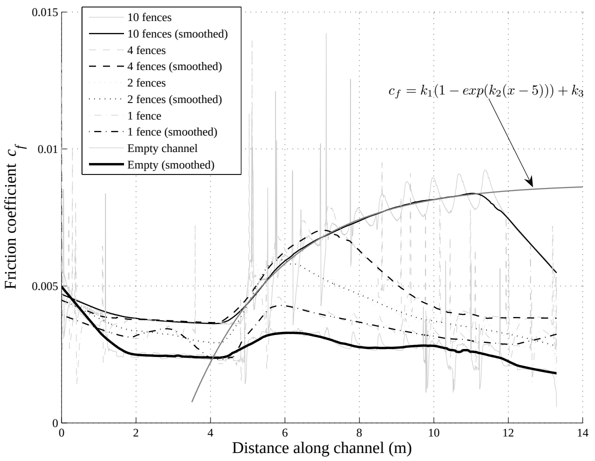

Figure 9: Variation of bed friction coefficient with distance along channel. Friction coefficient c_f is referred to the local depth-averaged flow speed.

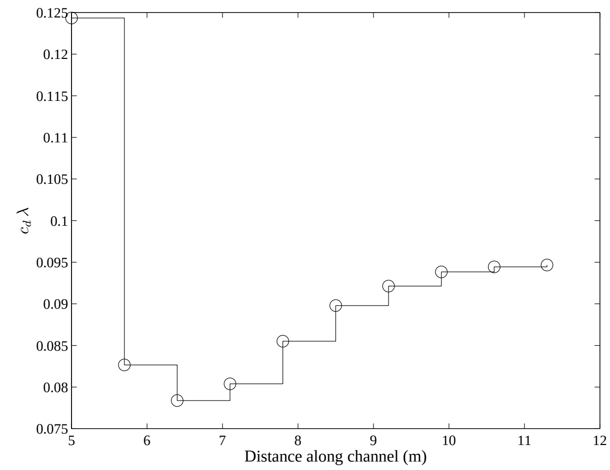

Figure 10: Variation of area-averaged fence drag $c_d\lambda$ with distance along channel. Drag coefficient is referred to the local depth-averaged flow speed.

Reasonable agreement in velocity profile was found above and on the centre-line of the fences, but was poorer below.

3. The CFD model was extended to an array of ten fences to examine the degree of convergence on equilibrium values for an array with an infinite number of fences. The area-averaged drag coefficient of the fences $c_d\lambda$ converged to 0.0947 ± 0.0002. The variation of bottom friction coefficient with distance from the first fence was fitted to a build-up exponential curve which predicted an equilibrium value $c_f = 0.00873$ with a 95% confidence interval of 5×10^{-5}.

4. The new model was compared with the predicted equilibrium values from the CFD model, giving an RMS difference of 0.0127 m/s over the interval $0.2 \leq z \leq 0.3$ when compared to the profile 10.6 m downstream from the CFD results.

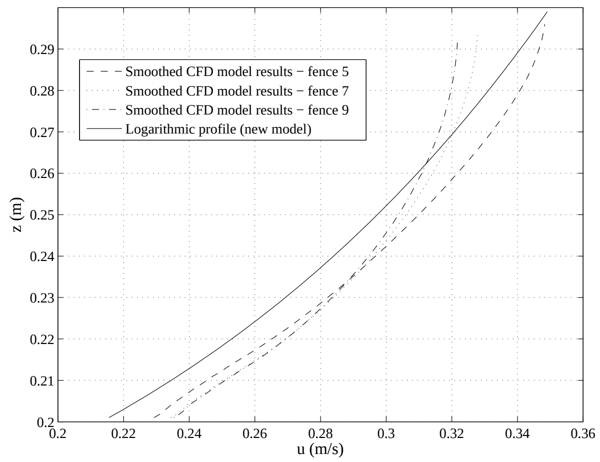

Figure 11: Comparison of velocity profiles above fences from smoothed CFD results with prediction from new model

5. There is more work to do, both computational and experimental in linking the bottom friction and the lower velocity profile to the velocity on the centre-line and the upper velocity profile, in order to make the model useful for predicting velocity deficit in a large array as a function of spacing and bed roughness.

References

[1] L. S. Blunden and A. S. Bahaj. Flow through large arrays of tidal energy converters: is there an analogy with depth limited flow through vegetation? In A. A. M. Sayigh, editor, *Tenth World Renewable Energy Congress*, Glasgow, 2008. Elsevier.

[2] P. B. S. Lissaman. Energy effectiveness of arbitrary arrays of wind turbines. *Journal of Energy*, 3(6):323–328, 1979.

[3] D. J. Milborrow. The performance of arrays of wind turbines. *Journal of Industrial Aerodynamics*, 5(3-4):403–30, 1980.

[4] L. J. Vermeer, J. N. Sorensen, and A. Crespo. Wind turbine wake aerodynamics. *Progress in Aerospace Sciences*, 39(6-7):467–510, 2003.

[5] C. Garrett and P. Cummins. The power potential of tidal currents in channels. *Proc. R. Soc. Lond. A*, 461(2060): 2563–2572, 2005.

[6] S. Frandsen, R. Barthelmie, S. Pryor, O. Rathmann, S. Larsen, J. Hojstrup, and M. Thogersen. Analytical modelling of wind speed deficit in large offshore wind farms. *Wind Energy*, 9(1-2):39–53, 2006.

[7] G. Sutherland, M. Foreman, and C. Garrett. Tidal current energy assessment for Johnstone Strait, Vancouver Island. *Proceedings of the Institution of Mechanical Engineers, Part A: Journal of Power and Energy*, 221(2): 147–157, 2007.

[8] L. S. Blunden and A. S. Bahaj. Effects of tidal energy extraction at Portland Bill, southern UK predicted from

a numerical model. In A. Falcão, editor, *Seventh European Wave and Tidal Energy Conference*, Porto, Portugal, 2007.

[9] I. G. Bryden, S. J. Couch, A. Owen, and G. Melville. Tidal current resource assessment. *Proceedings of the Institution of Mechanical Engineers, Part A: Journal of Power and Energy*, 221(2):125–135, 2007.

[10] M. R. Raupach, R. A. Antonia, and S. Rajagopalan. Rough-wall turbulent boundary layers. *Applied Mechanics Reviews*, 44(1):1, 1991.

[11] P. S. Jackson. On the displacement height in the logarithmic velocity profile. *Journal of Fluid Mechanics*, 111: 15–25, 1981.

[12] U. Stephan and D. Gutknecht. Hydraulic resistance of submerged flexible vegetation. *Journal of Hydrology*, 269(1-2):27–43, 2002.

[13] E Bossanyi, C. Maclean, G. E. Whittle, P. D. Dunn, N. H. Lipman, and P. J. Musgrove. The efficiency of wind turbine clusters. In *Third international symposium on wind energy systems*, pages 401–416, Technical University of Denmark, Lyngby, 1980. BHRA, Cranfield, UK.

[14] B. G. Newman. Spacing of wind turbines in large arrays. *Energy Conversion*, 16(4):169–171, 1977.

[15] S. Frandsen. On the wind speed reduction in the center of large clusters of wind turbines. *Journal of Wind Engineering and Industrial Aerodynamics*, 39(1-3):251–265, 1992.

[16] J. Højstrup, M. S. Courtney, C. J. Christensen, and P. Sanderhoff. Full scale measurements in wind turbine arrays. Nørrakær Enge II. CEC/JOULE. Technical Report Risø-I-684(EN), Risø National Laboratory, March 1993.

[17] H. M. Nepf and E. R. Vivoni. Flow structure in depth-limited, vegetated flow. *Journal of Geophysical Research*, 105(C12):28547–57, 2000.

[18] U. Neumeier. Velocity and turbulence variations at the edge of saltmarshes. *Continental Shelf Research*, 27(8): 1046–1059, 2007.

[19] A. S. Bahaj, L.E. Myers, M.D. Thomson, and N. Jorge. Characterising the wake of horizontal axis marine current turbines. In A. Falcão, editor, *Seventh European Wave and Tidal Energy Conference*, Porto, Portugal, 2007.

[20] R. W. MacDonald. Modelling the mean velocity profile in the urban canopy layer. *Boundary-Layer Meteorology*, 97(1):25–45, 2000.

[21] T. Bentham and R. Britter. Spatially averaged flow within obstacle arrays. *Atmospheric Environment*, 37(15):2037–2043, 2003.

[22] A. R. Campbell, J. H. Simpson, and G. L. Allen. The dynamical balance of flow in the Menai Strait. *Estuarine, Coastal and Shelf Science*, 46(3):449–455, 1998.

[23] A. J. Elliott. The boundary layer character of tidal currents in the eastern Irish sea. *Estuarine, Coastal and Shelf Science*, 55(3):465–480, 2002.

[24] K. Dyer. *Coastal and Estuarine Sediment Dynamics*. John Wiley & Sons, Chichester, 1986.

[25] V. T. Chow. *Open-channel hydraulics*. McGraw-Hill, 1959.

[26] R. Wooding, E. Bradley, and J. Marshall. Drag due to regular arrays of roughness elements of varying geometry. *Boundary-Layer Meteorology*, 5(3):285–308, 1973.

[27] M. E. Harrison, W. M. J. Batten, L. S. Blunden, L. E. Myers, and A. S. Bahaj. Comparisons of a large tidal turbine array using the boundary layer and field wake interaction models. In *Second International Conference on Ocean Energy (ICOE 2008)*, Brest, 2008.

[28] G. Voulgaris and J. H. Trowbridge. Evaluation of the Acoustic Doppler Velocimeter (ADV) for turbulence measurements. *Journal of Atmospheric and Oceanic Technology*, 15(1):272–289, 1998.

[29] ANSYS®. ANSYS academic solutions. `http://www.ansys.com/academic/`, 2009.

[30] F. R. Menter. A comparison of some recent eddy-viscosity turbulence models. *Journal of Fluids Engineering*, 118(3):514–519, 1996.

[31] L. E. Myers, A. S. Bahaj, G. Germain, and J. Giles. Flow boundary interaction effects for marine current energy conversion devices. In A. A. M. Sayigh, editor, *Tenth World Renewable Energy Congress*, Glasgow, 2008. Elsevier.

[32] P. J. H. Builtjes and D. J. Milborrow. Modelling of wind turbine arrays. *Precision Engineering*, pages 417–430, 1980.